Journal of Power Sources 241 (2013) 467–476

Contents lists available at SciVerse ScienceDirect

Journal of Power Sources

journal homepage: www.elsevier.com/locate/jpowsour

Homogenized mechanical properties for the jellyroll of cylindrical Lithium-ion cells

Tomasz Wierzbicki [1], Elham Sahraei*

Impact and Crashworthiness Lab, Massachusetts Institute of Technology, 77 Massachusetts Ave, Room 5-218A, Cambridge, MA 02139, USA

HIGHLIGHTS

- A method was developed to estimate the structural strength of cylindrical cells.
- The procedure was illustrated on a commercial 18650 lithium-ion cell.
- A finite element model of the cell was then created.
- The model was validated in local crush scenarios.
- The model predicts loads, deformation, and possibility of short circuit.

ARTICLE INFO

Article history:
Received 2 January 2013
Received in revised form
19 April 2013
Accepted 23 April 2013
Available online 9 May 2013

Keywords:
Lithium-ion cell
Cylindrical battery
Mechanical properties
Finite element

ABSTRACT

A hybrid experimental/analytical approach was developed for extracting the average mechanical properties of cylindrical Li-ion cells. By using the principle of virtual work, and estimating the load transfer mechanism inside the cell, the stress–strain relation for the jellyroll was calculated for the case where the cell was crushed between two flat plates. The procedure was illustrated on an example of a commercial 18650 cell. A finite element model of the cell was then developed using the crushable foam material in LS Dyna. The model calibrated with this method closely predicts kinematic of the cell during two different load cases used for validation. These cases include local crush by a hemispherical punch and indentation by a rigid rod. The load and displacement during deformation, as well as onset of electric short circuit observed from experiments were closely predicted from simulations. It was found that the resistance of the cell comes primarily from the jellyroll. Additional analytical calculations showed that the shell casing and the end-caps provide little contribution to the overall crash resistance of the cell in the loading cases studied in this paper.

1. Introduction

Individual Lithium-ion battery cells consist of a jellyroll packaged inside a soft pouch or hard steel or aluminum shell casing. The jellyroll, in turn is composed of layers of electrode/separator assembly, which is rolled, or stacked inside the casing, depending on the form factor of the battery (pouch, cylindrical, and prismatic). The components of the electrode/separator assembly are the coated copper, and aluminum foils that are kept apart by a polymeric separator. The coating itself is a mixture of active powders with a binder and soaked in electrolyte. Typical thickness of coated aluminum or copper foils is about 0.1–0.2 mm. The metal foils contribute to about 10–15 μm each, and the remaining thickness comes from graphite or lithium metal oxide (or phosphate) powder. The thickness of the polymeric separator is also in the order of 10–25 μm. In a typical consumer electronic, lithium-ion cell can have about 20 layers (see Fig. 1). The number of layers for the automotive size cells could be much larger. It is evident that the battery cells are spanning at least three orders of magnitude in the length scale.

The mechanical response of individual components of the cell under certain loading conditions was studied by several authors. Shim et al published results of uniaxial tensile tests on copper and aluminum foils to model blanking of current collectors and formation of burrs that may affect performance of the battery under charging and discharging cycles and accidental loads [1]. The tensile strength of the active material is related to strength of the binder and it is generally, relatively low. Ways of increasing the tensile strength were studied by Liu et al. [2]. They performed tensile tests on coated cathode and reported a fivefold increase in

* Corresponding author. Tel.: +1 617 324 5025.
E-mail addresses: wierz@mit.edu (T. Wierzbicki), elhams@mit.edu (E. Sahraei).
[1] Tel.: +1 617 253 2104; fax: +1 617 253 8689.

0378-7753/$ – see front matter © 2013 Elsevier B.V. All rights reserved.
http://dx.doi.org/10.1016/j.jpowsour.2013.04.135

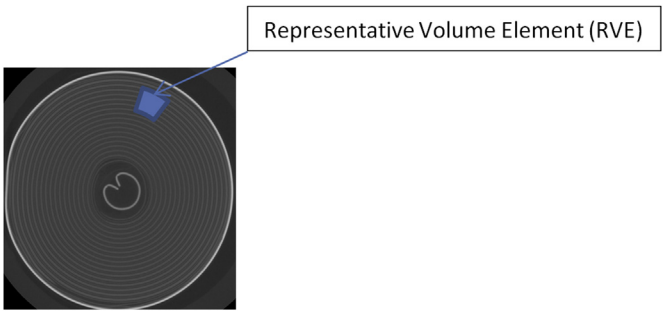

Fig. 1. CT-Scan of a cross-section of an 18650 cylindrical cell.

the tensile strength by adding short carbon nanofibers to the matrix. Sheidaei et al studied properties of polypropylene separators in tension, and found a very strong anisotropy [3]. The anisotropic structure of this polymer is due to the manufacturing technique that produces porous sheets through crazing. Results from Venugopal et al. as well as Anand and Di Leo also confirm anisotropic behavior of the separator [4,5]. All the above publications have shown an order of magnitude difference between the strength of separator in machine direction versus transverse direction. Breaking strain and the strength of polymeric separators was reported by Djion et al. [6].

No publication could be found in the literature that presents a comprehensive study of mechanical properties of all five components of the jellyroll. Likewise, no effort has been reported in literature to integrate the properties of the five layers into one homogenized representative volume element (RVE). While, this line of research is being conducted by the present investigating team, a different approach is proposed here to determine average constitutive properties of the RVE. In a small pouch cell, the length and width of the cell are about an order of magnitude larger than its thickness. Also, the small size of the cells allows using a standard 200 KN testing machine to test the cell under compression without a need to cut a specimen. The compression tests on these cells produce a uniaxial strain condition that would directly give the stress strain of the jellyroll, as reported by Sahraei et al. [7]. The properties found with this method were sufficient to model the behavior of batteries in several loading conditions.

It is far more difficult to determine the compressive properties of the jellyroll in cylindrical cells, because there is not any simple test in which the state of stress and strain is uniform and could be measured directly. In fact, there are always regions of compressive, tensile, and shear stress in the jellyroll in even simple loading conditions. In order to overcome this difficulty, a hybrid analytical/experiment technique is proposed in this paper. This method consists of defining the average stress and strain in the deforming region as a function of the global measurable quantities such as load and displacement. Then, by comparing the analytical prediction with quantities measured from experiments, the constitutive behavior of the jellyroll in compression can be uniquely determined. For the above calibration procedure, lateral compression of a cylindrical cell between two plates was chosen. The method is quite general and is applicable to various loading situations on the cell. Two types of validation tests were conducted by performing local indentation by a cylindrical and a hemispherical punch. In both cases, very good correlation between the experimental and measured response was found. With a proper selection of the tensile cut-off value, the peak force corresponding to jellyroll failure and onset of electric short circuit is also predicted correctly.

Until recently the battery development was supported by testing alone. The present analysis provides a valuable contribution to the development of a reliable computational model of cylindrical cells, which is an extension of previously published results of the same team for pouch and cylindrical batteries [8,9].

2. General formulation

2.1. Discussion of 3D constitutive model

The most general constitutive equations to describe the jellyroll were discussed by Greve and Fehrenbach [10]. The authors distinguish between plastic flow and fracture. In order to predict failure of the jellyroll, the Coulomb–Mohr model was used by Greve and Fehrenbach. For the plastic flow, a special function with five parameters was suggested. The function predicts a nonlinear transition from the purely elastic range to the constant stress plateau followed by densification and stiffening. For all practical purposes, this model has been shown to be equivalent to a much simpler model which is proposed in the present paper.

The previous work of the present team has shown that the model of crushable foam from LS Dyna library of materials may be used to model behavior of the jellyroll under various loading conditions. In this model, the volumetric stress, σ_v, is a nonlinear function of the volumetric strain, ε_v.

$$\sigma_v = f(\varepsilon_v) \tag{1}$$

There is an extensive literature on constitutive modeling of crushable foams (see for example, [11–18]). In most polymeric and metallic foams, the Poisson ratio is very small. The presently considered electrode/separator assembly consists predominantly of graphite and Li-metal oxide coating, a porous structure as well, and thus is assumed to have a very small Poisson ratio. Furthermore, the present model is sufficiently general, and it allows inputting different properties in tension and compression. Typical polymeric and even metallic foams are characterized by the stress–strain shown in Fig. 2a. There are two differences between the standard polymeric and metallic foam and the jellyroll of the Li-ion batteries. First, the coated material takes little tensile strength before failure. This could be represented by a tensile cut-off value, represented by the parameter σ_f. The other difference is that because of the nature of the jellyroll, which consists of stack or wound layers, there is no detectable linear range in the stress–strain curve under compression. The presently proposed model is illustrated in Fig. 2b, and it will be calibrated through a single test generating compressive stresses and strains. The tensile properties are taken from the literature, where tensile tests are reported for coated electrode and for separators [1–3].

2.2. Discussion of stress and strain state

In general, material properties should be determined from tests on specimens with uniform, homogenous state of stress and strain. In the present stage of research, it is possible to determine the homogenous properties of the internal structure of the batteries, which are averaged over a number of individual layers of the electrode/separator assembly inside a representative volume element. In small pouch batteries subjected to compression between the flat rigid plates, the uniaxial state of strain develops. The logarithmic stress, $\varepsilon_{\log}$, in the through thickness direction is

$$\varepsilon_{\log} = \ln\frac{H}{H_0} = \ln\frac{H_0 - w}{H_0} = \ln\left(1 - \frac{w}{H_0}\right) \tag{2}$$

where H_0 and H denote the initial and deformed thickness and w is the amount of compression that will be referred to as the crush

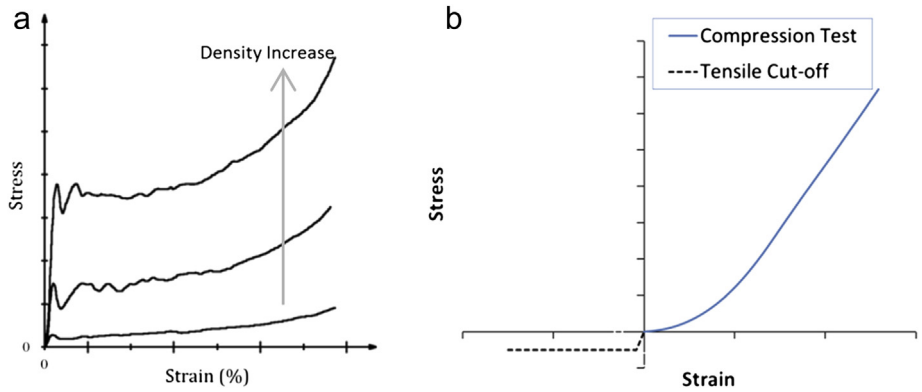

Fig. 2. Stress–strain curve from an aluminum foam (left, a), and a lithium-ion cell (right, b).

distance. In the limiting case of small displacements, the engineering strain, ε, is recovered from Eq. (2) as

$$\varepsilon = \frac{w}{H_0} \tag{3}$$

Because the batteries resist loading mainly in compression, compressive stresses and strains are considered positive in Eq. (3) and thereafter.

In compression of pouch cells between the flat rigid plates, the uniaxial state of strain develops and all other components of the strain tensor are zero. Therefore, the through thickness strain is also a volumetric strain. The area, A, of the battery remains approximately constant during loading so that the engineering and Cauchy stress in the direction of compression are the same

$$\sigma = \frac{P}{A} = \frac{P}{2bL} \tag{4}$$

where P is the total load and $2b$ and L denote the width and length of the cell, see Fig. 3. In uniaxial compression, three in-plane reaction stresses develop, the vertical stress is measured from Eq. (4), but it is difficult to measure in-plane compressive stresses. A series of compression tests on pouch cells were performed earlier by the present team and the results were reported in [7]. The maximum force generated during those tests reached almost 200 KN load limit of the MTS loading frame. The difficulty is that large pouch batteries used for PHEV and EV may have the planar area up to 20 times larger. Testing them with the same method would require access to massive 4000 KN load frames, or would require cutting smaller rectilinear samples.

Determination of mechanical properties of cylindrical cell is not straight forward, because the stress state inside the cell is highly inhomogeneous, changing from point to point. Only average stresses and strains could be found from one test, and for that purpose a number of assumptions must be made. The present derivation is based on careful observation of the shape of the deforming jellyroll, without end-caps, reported in [7–9,19]. In addition, an FE simulation was performed where the layered structure of the cell was modeled by a combination of solid and shell elements. There were 18 layers, and the interface between those layers was modeled as frictionless. To decide about proper assumptions for this study, the contour of compressive stresses in z direction during compression of the layered jelly-roll was plotted in Fig. 4. In this figure, the convention is that red color indicates no compression stresses (or small tensile stresses), while the yellow, blue, and green regions are the areas of compression.

From the careful observation of the deforming cells during tests and the above numerical simulation of layers of jellyroll, the following conclusions can be drawn:

- The total length of the cylindrical cell remains constant so that plane strain develops in the cross-section
- The cylinder of the original radius R is flattened, where the flat contact length $2b$ is flanked by two semicircles of the radii, r, see Fig. 5. Devoting $\delta = R - r$, the total crush distance becomes $w = 2\delta$.
- The cross-sectional length of the shell casing remains constant which means the inextensibility in the hoop direction
- Only the central rectangular part of the jelly-roll under the punch takes the compressive load. The stress in the two outside semicircles is very small. This is the region that the bending of individual winds takes place.

The above conclusions are used in the next section to justify a set of assumptions and to drive the local average stress–strain curve of the interior of the cell from the measured global response.

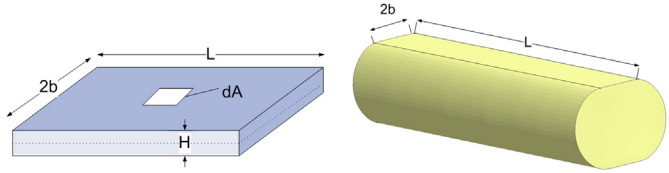

Fig. 3. Schematic of a pouch cell (left), and a cylindrical cell (right).

3. The principle of virtual work

The constitutive equation of the jelly-roll will be determined from the lateral compression of the cell between rigid plates.

The quantities that could be measured in the calibration experiments are the total force P versus the cross-head displacement w (see Fig. 6). Therefore, the objective of the theoretical developments is to relate the internal stresses and strains to the measured quantities. The starting point in derivation is the principle of virtual work.

$$P\dot{w} = 4\int_V \sigma_{ij}\dot{\varepsilon}_{ij}\,\mathrm{d}V \tag{5}$$

where σ_{ij} and $\dot{\varepsilon}_{ij}$ are components of the macroscopic stress and strain rate tensors in the RVE, where dV denotes the incremental volume of the cell. There are two planes of symmetry, so it is sufficient to consider only a quarter of the cell. Therefore, in Eq. (5), V

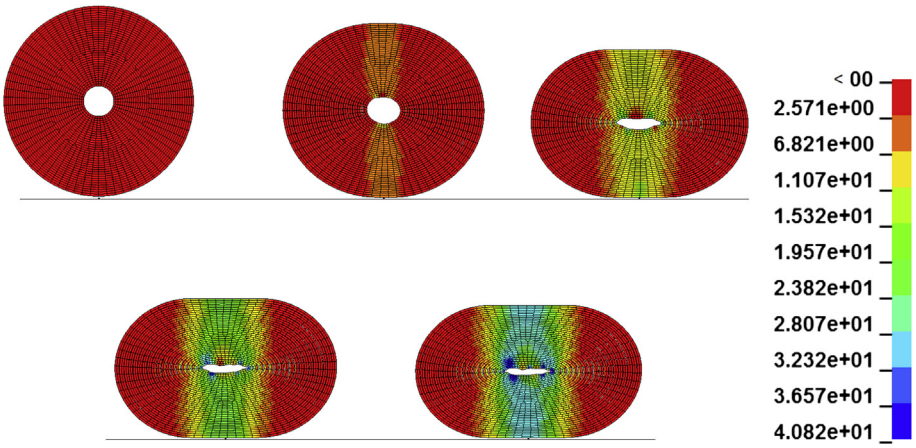

Fig. 4. A cross-section model of layers of an 18650 cell.

denotes the volume of the deforming material in one quarter of the cell. Because, the length of the cylinder is much larger than its radius, the plain strain prevails inside the cell, so that $dV = LdS$, where dS is the area element in the cross-section. The cross-section S is composed of two parts, $S = S_1 + S_2$. Here S_1 is the rectangular area between the two flat parts of the cross-section. The two semicircular parts of the area are denoted by S_2, and the corresponding rate of energy dissipation is small as demonstrated in Section 5. Therefore, from now on the integration is performed only over S_1.

Even though the initial geometry of the cell calls for the description in the cylindrical coordinate system (r, θ, z), the contact zone is flat, so that the rectangular coordinate system (x, y, z) will be used. In the plane strain case, three components of the strain rate tensor vanishes

$$\dot{\varepsilon}_{zx} = \dot{\varepsilon}_{zy} = \dot{\varepsilon}_{zz} = 0 \tag{6}$$

and the remaining components of the strain rate tensor are

$$\dot{\varepsilon}_{ij} = \begin{vmatrix} \dot{\varepsilon}_{xx} & \dot{\varepsilon}_{xy} & 0 \\ \dot{\varepsilon}_{yx} & \dot{\varepsilon}_{yy} & 0 \\ 0 & 0 & 0 \end{vmatrix} \tag{7}$$

In the layered structure of the battery interior, shear forces transmitted from layer to layer are assumed to be small so that $\sigma_{xy} = \sigma_{yx} = 0$, since set of electrode separator assembly can slide with respect to one another. The delamination of the layers in y direction in the semicircular zones leads to small stress in y direction for the S_1 section, $\sigma_{yy} = 0$. With all the above assumptions, the internal rate of work in the cell reduces to

$$P\dot{w} = 4L \int_{S_1} \sigma_{xx}\dot{\varepsilon}_{xx}\, dS \tag{8}$$

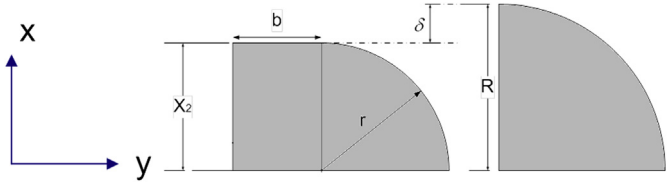

Fig. 5. Geometry of cell deformation under lateral compression.

The stress and strain rates change from point to point and with punch travel. The only way to drive the homogenized stress–strain curve in the RVE is to introduce a spatial average of both stresses and strains. According to the mean value theorem

$$L \int_{S_1} \sigma_{xx}\dot{\varepsilon}_{xx}\, dS = LS_1\sigma_{av}\dot{\varepsilon}_{av} \tag{9}$$

Solving Eqs. (8) and (9) for σ_{av}, one gets

$$\sigma_{av} = \frac{P\dot{w}}{4LS_1\dot{\varepsilon}_{av}} \tag{10}$$

In the next step the relation between $\dot{w}$ and $\dot{\varepsilon}_{av}$ must be established. Defining the strain rate $\dot{\varepsilon}_{xx}$ as the gradient of the velocity field in the x-direction

$$\dot{\varepsilon}_{xx} = \frac{d\dot{u}_x}{dx} \tag{11}$$

The average strain rate over the surface S is

$$\dot{\varepsilon}_{av} = \frac{1}{S_1} \int_S \dot{\varepsilon}_{xx}\, dS \tag{12}$$

The product of the two terms in the denominator of Eq. (10) is

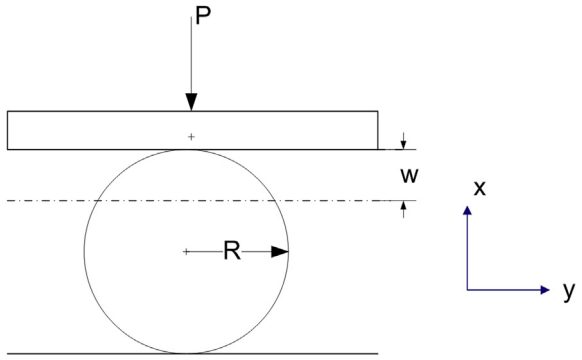

Fig. 6. Compression of a cell between two flat plates.

$$S_1\dot{\varepsilon}_{av} = \int_0^o \int_{x_1=0}^{x_2} \frac{d\dot{u}_x}{dx}\, dx\, dy = \int_0^o [\dot{u}_x(x_2) - \dot{u}_x(0)]\, dy \tag{13}$$

where $x_1 = 0$ is the plane of symmetry of the cell, and x_2 is the moving interface of the flattened cell and the compression plate

$$\dot{u}_x(x_2) - \dot{u}_x(0) = \dot{\delta} = \frac{\dot{w}}{2} \tag{14}$$

Now, the integration in Eq. (13) can be performed to give

$$S_1\dot{\varepsilon}_{av} = \dot{\delta}b \tag{15}$$

The shell casing is inextensible in the hoop direction and so is the outmost electrode/separator layer

$$\frac{\pi}{2}R = \frac{\pi}{2}r + b \tag{16}$$

It follows that the contact width b is linearly related to the crush distance w by

$$b = \frac{\pi}{2}\delta = \frac{\pi}{4}w \tag{17}$$

The final expression for the average strain rate is

$$S_1\dot{\varepsilon}_{av} = \frac{\pi}{8}w\dot{w} \tag{18}$$

Substituting the above result into Eq. (10), the average stress as a function of the measured force and displacement is

$$\sigma_{av} = \frac{2P(w)}{\pi L w} = \frac{P}{2bL} \tag{19}$$

It is interesting to note that rigorous application of the principle of virtual work gives the same expression for σ_{av} as simply dividing the compressive force by the current contact area between the cell and the plate, $2bL$.

The last step in the derivation is to find a relation between the total crush distance w and the average strain. This can be accomplished by integrating the expression for $\dot{\varepsilon}_{av}$, given by Eq. (18) in time

$$\varepsilon_{av} = \int_0^t \dot{\varepsilon}_{av}\, dt = \int_0^t \frac{\pi}{8}\frac{w\dot{w}}{S_1}\, dt \tag{20}$$

where the area of the deforming zone is approximated by

$$S_1 = Rb = \frac{\pi}{4}Rw \tag{21}$$

After integration, Eq. (20) yields a very simple expression

$$\varepsilon_{av} = \frac{w}{2R} \tag{22}$$

Eliminating the crush distance, w, between Eqs. (19) and (22) one arrives at the final expression between the average stress and strain in the RVE.

4. Example application

The general framework developed in the previous section could be applied to any type of cylindrical cell. As an application of the above calibration procedure, the properties of jellyroll will be determined for a commercial 18650 cylindrical cell. Only one test is needed for calibration of this model. It consists of a lateral crash of a cell between two rigid plates. We have performed such tests on fully discharged cells, with end-caps removed, and the results were reported in [9]. The measured force–displacement relations for the first 6 mm of crush distance in the two tests are shown in Fig. 7.

There is always some uncertainty in determining the origin of the force–displacement relation, because of the presence of unavoidable gaps between outside shell casing and the jellyroll as well as individual layers. Considering the above, a goof fit of the crush response is provided by the cubic equation:

$$P(w) = Bw^3 \tag{23}$$

where $B = 140$ N/mm^3. The total measured force comes from the contribution of the jellyroll and the shell casing. The outer shell is, in the present case, an open ended thin cylinder. The contribution of the shell casing is quantified in the subsequent section, and is shown to be only a small percentage of the total resistance force. Therefore, it is neglected in the present calibration procedure. Substituting Eq. (24) into the expression for the average stress, Eq. (19), one gets

$$\sigma_{av} = \frac{2}{\pi}\frac{Bw^2}{L} \tag{24}$$

Using Eq. (22), the cross-head displacement, w, can be eliminated and the final expression for the stress–strain relation of the RVE of the jelly-roll becomes

$$\sigma_{av} = \frac{8}{\pi}\frac{BR^2\varepsilon_{av}^2}{L} \tag{25}$$

The input values to Eq. (25) corresponding to 18650 cell are given in Table 1. It should be noted because the two end-caps with the adjacent assembly were removed before the test, the total length of the cylinder is 58 mm rather than nominal value of 65 mm.

With the above values, the compressive strength of the jellyroll is the following parabolic function of the stress

$$\sigma = c\varepsilon_{av}^2[\text{MPa}], \quad c = 498\ \text{MPa} \tag{26}$$

It is interesting to compare the present constitutive equation for a cylindrical cell with that measured from the compression test of small commercial pouch batteries of same chemistry, discussed in

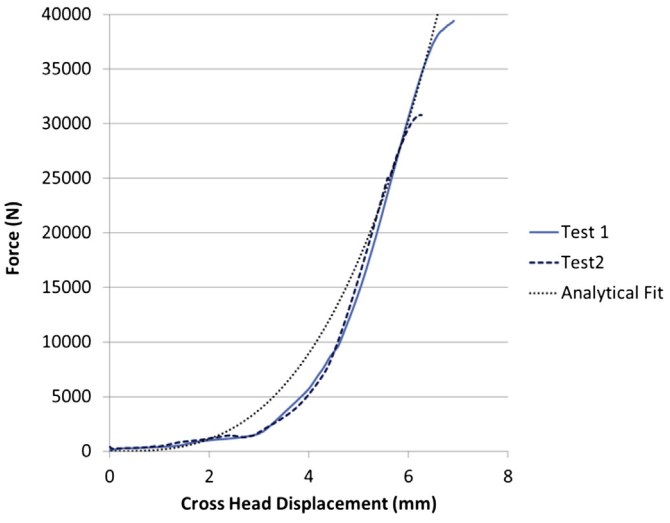

Fig. 7. Measured load–displacement, and analytical fit, compression between two flat plates.

Table 1
Properties of 18650 cylindrical cell.

R (mm)	L (mm)	B (N/mm^3)
9	58	140

the introduction [7,8]. The solid line in Fig. 8 corresponds to the pouch cell, while the prediction of Eq. (26) is represented by the dotted line.

The two lines are close to each other, which is not surprising, since most of the compressive resistance of the electrode/separator assembly come from the active powders of Lithium metal oxide and graphite. Both the pouch cells tested by present authors [8], and the cylindrical cells have the same $LiCoO_2$/graphite active ingredients. A word of caution should be offered for the end users of the present computational models. As new types of batteries are entering the market with improved or different chemistry, so for each case, the constitutive equation should be properly calibrated for practical applications.

5. Other contributions to the crush resistance

The shell casing is a deep drawn cylindrical structure made of aluminum or steel. It resembles a thin metal can used for various types of beverages. The crushing strength of the shell casing comes from the lateral cylindrical part and two end-caps. Only one cap is an integral part of the drawn casing. The other one is added on after inserting the jellyroll. It contains a plastic insulation ring and its strength is very small. The lateral crushing of an empty tube (with end-caps removed) was studied by DeRuntz and Hodge [20] who derived a simple closed-form solution on the relation between the crushing force, P_{shell}, and the crush distance

$$P_{\text{shell}} = \sigma_0 t^2 \frac{L}{R} \frac{1}{\sqrt{1-\left(\frac{w}{2R}\right)^2}} \tag{27}$$

where σ_0 is the average flow stress of the shell casing material (500 MPa), and t is the thickness of shell casing (0.16–0.3 mm). The tube resistance is predominantly due to bending.

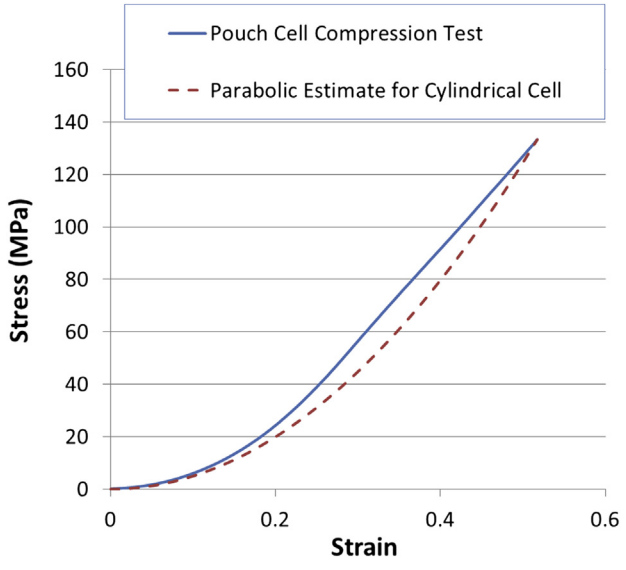

Fig. 8. Stress–strain relation for a pouch cell versus the one calibrated for 18650 cylindrical cell.

The force is an increasing function of the displacement, w. When the cylinder is flattened by one half of its original diameter, $w = R$, the resistance of shell casing becomes equal to 95 190 N. This value is 0.3–0.6% of the peak force, and could be neglected in the calculations.

The energy absorption of bulkheads (end-caps) was studied experimentally and theoretically by Yahoui [21]. Several different crush modes were considered. It was shown that the upper bound on the resistance of the end cap is expressed in terms of σ_0, thickness of end cap, t_c, and R by

$$P_{\text{end cap}} = 3\sigma_0 t_c^{1.75} R^{0.25} \tag{28}$$

Both bending and membrane resistance is invoked, so the resistance is proportional to $t_c^{1.75}$, instead of t_c^2, as in the case of the lateral portion of the shell casing. Again, by putting the input values for the geometrical and material parameters, the estimated contribution of one end cap will be 316 N, which is about 1% of the total resisting force from test.

Bending resistance of the *jelly-roll.* In Section 2, two resisting mechanisms of a cylindrical cell were identified: uniaxial compression of the central compressive zone and bending resistance of the layers outside the compressive zone.

The photos from the deforming jellyroll as well as numerical simulations (Fig. 2) prove that in the two semicircular zones, there is a delamination of individual layers, so they do not interact with one another. Therefore, the total resisting force, P_{bending}, is a sum of the resistance of individual rings/cylindrical panels, P_i:

$$P_{\text{bending}} = \sum_{i=1}^{N} P_i \tag{29}$$

where N is the total number of windings in the cell. Each layer is inextensible, so that its resistance is derived from the bending action only.

Consider a half of a cylinder with the length L and the instantaneous radius r_i (see Fig. 9). The resistance force P_i is determined from the principle of virtual work

$$\frac{P_i}{2}\dot{w} = \int_A \left|M\dot{K}\right| \mathrm{d}A \tag{30}$$

The curvature, K, and its rate are

$$K = \frac{1}{r_i}; \quad \dot{K} = \frac{\dot{r}_i}{r_i^2} \tag{31}$$

The bending moment per unit width is found from the definition

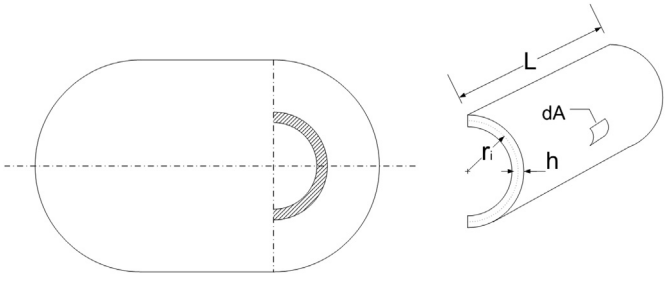

Fig. 9. Geometry of the semicircular section of an individual layer during deformation.

$$M = 2\int_0^{h/2} \sigma z \, dz \tag{32}$$

where z is measured from the neutral axis of the layer. It is assumed that the compressive and tensile properties of the electrode coating are the same and are given by Eq. (26), $\sigma = c\varepsilon_{av}^2$. This gives an upper bound resistance, because in reality the active anode material with a binder or the graphite is much weaker in tension than compression. Also the diameter of the central mandrel, which reduces the cell's strength, is not taken into account.

With the Euler–Bernoulli assumption, $\varepsilon = zK$, considering the bending stress across the length of a given layer from unrolled condition:

$$\sigma_i(z) = c\frac{z^2}{r_i^2} \tag{33}$$

and the bending moment becomes

$$M_i = \frac{ch^4}{32r_i^2}\left[\frac{\text{Nm}}{\text{m}}\right] \tag{34}$$

The resulting crush resistance of the i-th layer is

$$P_i = \frac{\pi}{32}cL\frac{h^4}{r_i^3} \tag{35}$$

The radius of the i-th layer is $r_i = ih$, and the total crush resistance of the cell outside the compressive zone is given by

$$P = \frac{cLh\pi}{32}\sum_{i=1}^{N}\frac{1}{i^3} \tag{36}$$

The series converges rapidly and for $N = 18$ its sum is equal to 1.202. The final expression for P in the initial configuration is

$$P = 0.12cLh \tag{37}$$

For the crush distance equal to the radius, the above equation should be multiplied by $2/\sqrt{3}$. Taking $h = 0.1$ mm, the bending resistance of the semicircular sections of the jellyroll is 0.368 kN. This is less than 1% of the maximum resistance of the cell.

6. Validation

It is very important that the validation of the proposed model be done on a different type of test than the calibration. The constitutive equation of the jelly-roll was determined in the previous section from a compression test between two flat plates. The prediction of the calibrated constitutive law has been validated with two additional types of tests, indentation with a rigid rod, and local crush with hemispherical punch. In the two chosen cases, tensile stresses appear in the cell in addition to the compressive stresses, which make the whole analysis much more interesting.

6.1. Summary of the test results

A comprehensive set of tests on 18650 cylindrical cells was performed in our lab, and the results were published in [7,9]. Here only a short summary of the testing procedure is given. All the tests were performed on 90% discharged batteries, in order to prevent catastrophic thermal runaway of the cells. The remaining 10% charge was sufficient to monitor the voltage and detect sudden drops in voltage indicating substantial internal damage and onset of electric short circuit. A photograph of the experimental set-up is shown in Fig. 10.

Measured in the test were force, displacement, voltage, and temperature of the cell as a function of time. A typical output from the test is shown in Fig. 11. As displacement increases at a prescribed rate of 1 mm/min, the force is seen to increase in a parabolic manner, reaching a maximum, and dropping suddenly at a critical indentation depth. The voltage was constant up to this critical point and then suddenly dropped simultaneous with the drop in force. The deformation was stopped soon after the critical point. Each test configuration was repeated two times or more. The test trends were repeatable. Similar type of response was also observed in the case of local crush by a hemispherical punch, as can be seen from Figs. 4 and 5. Interested readers are referred to [7] for a complete report on the testing program.

6.1.1. Numerical simulations

A computational model of the 18650 cylindrical cell was composed of solid element for the jellyroll and shell elements for the metal casing. There were 29,106 solid elements and 11,133 shell elements in the model. Both shell and solid elements were of 0.8 mm in size. The jelly-roll material was modeled by crushable foam model from library of LS Dyna materials. Properties of the jellyroll are different in tension and compression. In this paper, we proposed using the test of compression of cylinder between two rigid plates, because the compressive state is dominant inside the jellyroll. The parabolic curve from Eq. (27) was used as the input for the crushable foam model in compression. The properties in tension are assumed to be linear up to a tensile cut of value, σ_f. This value is justified by comparing the values if tensile strength of separators, and coated electrodes reported in the literature with our own tests. Our experiments provided an approximate value of the tensile strength of the coated anode to be 10 MPa. A similar value was also found in [2] for cathode coating. The separator is a highly anisotropic structure, but it will fail always in the weakest direction. Sheidai et al., reported the tensile strength of the separator soaked in electrolyte in the transverse direction to be around 10 MPa [3]. A similar value was reported for dry separators by Anand and Cladio [5]. Therefore, in the present model of the jellyroll, the tensile cut-off value was assumed to be $\sigma_f = 10$ MPa.

The properties of the metal shell casing were extracted from testing of dogbone specimens cut from a commercial 18650 cell,

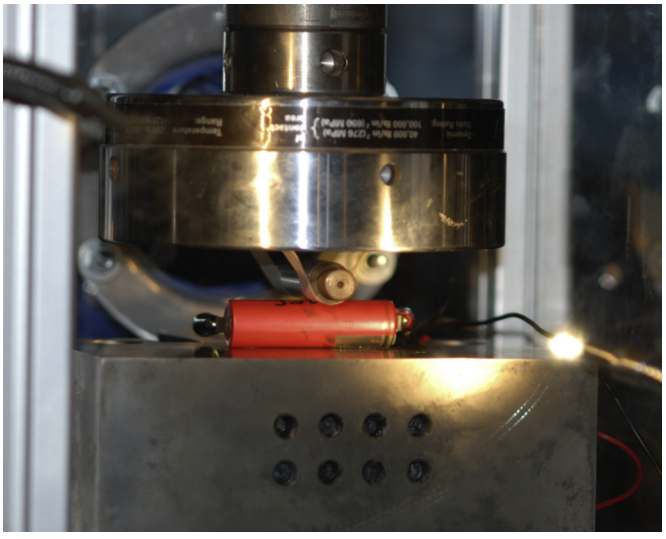

Fig. 10. Indentation of the cylindrical cell by a rigid rod, initial stage.

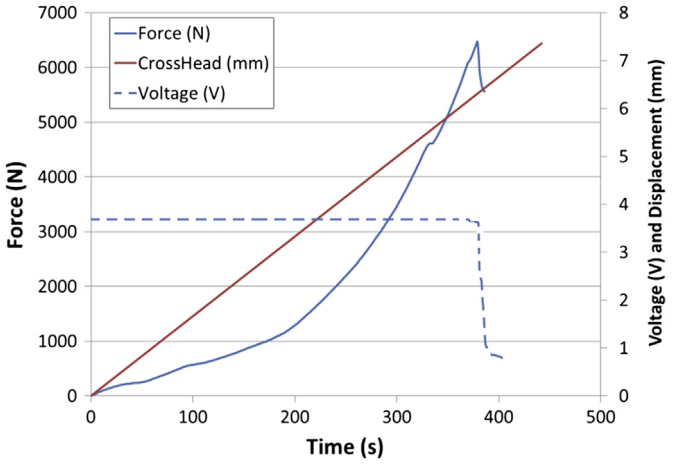

Fig. 11. Typical outputs from the indentation with rigid rod test.

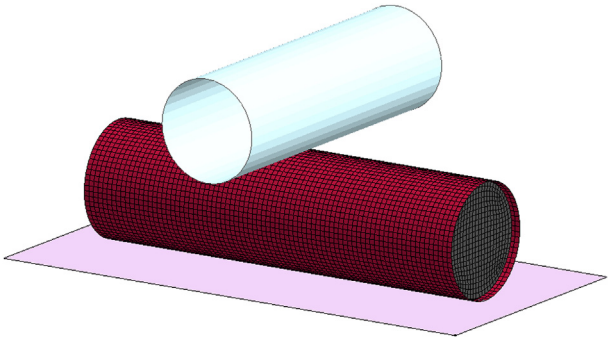

Fig. 12. The FE model of the indentation of a rigid punch, showing shell elements of casing in red, and solid elements of the jellyroll in gray color.

which was described in an earlier publication [9]. The model was simulated in two load scenarios, under an indentation with a rigid rod of 8 mm in radius (Fig. 12 and Fig. 13), and crush by a hemispherical punch of 6.4 mm in radius (Fig. 14). An "Entity Geometric" contact was used to simulate the contact of punches with the cell. A "Rigidwall" provided the flat support under the cell. LS Dyna version R5.1 was used for the simulations.

Fig. 13 shows the predicted force–displacement relation from simulation of indention by a rigid rod. This curve is compared to a test performed with same set-up. The results show that the simulation closely follows the load–displacement from the test. In addition, the peak load and its point of displacement corresponding to the onset of short circuit compares favorably with the measured values.

Fig. 14 depicts the simulation of crushing of the 18650 cell by a hemispherical punch. Again, the simulation is in a very close agreement with a corresponding test.

The numerical simulation proves the accuracy of the proposed calibration method, while uses only one test on cylindrical cells. One assumption has been made in the derivation that has to be verified. This is the assumption that the energy absorbing region under the punch can be approximated with a rectangle with decreasing height and increasing width. For that purpose, the same finite element model was used to simulate the compression of the cell between two flat plates (Fig. 15).

A sequence of snapshots of the deformed central-section, shown in Fig. 16, confirms the validity of the above assumption.

7. Discussion and conclusion

The present paper provides a step-by-step procedure to determine the compressive properties of the jellyroll in cylindrical cells. The proposed model was calibrated from one test, and validated against two other tests. It was shown that the proposed model predicts accurately the load–displacement curve, the magnitude of the peak load, and the corresponding indentation depth causing the onset of failure. In addition to the mechanical properties, monitored during the tests were the voltage and the temperature. In all cases, the drop of voltage that indicates the onset of electric short circuit coincided with a sudden drop of resisting force. The present model has proved to be useful in predicting the average response of the jellyroll to various types of loading histories. However, in reality, jellyroll is an alternating layered structure of electrode/separator assemblies. In order to predict which components of this assembly fails first, a more refined modeling is required, in which constitutive equation of each of the five components of the jellyroll should be considered with periodicity and appropriate continuity condition at the interfaces. This is the subject of a current research of the investigating team.

It is interesting to compare the compressive stress–strain curve given in this research with that of more complex model given by Greve and Fehrenbach 2012. In their model, they use a plastic flow rule in the form:

$$R(\bar{\varepsilon}^p) = \left[\sigma_{\text{plateau}} - \left(\sigma_{\text{plateau}} - \sigma_{\text{yield}}\right) * \text{Exp}\left[-\frac{\bar{\varepsilon}^p}{\bar{\varepsilon}_{\text{ref}}}\right]\right] \times \left[1 + s(\bar{\varepsilon}^p)^m\right] \quad \text{GPa} \tag{38}$$

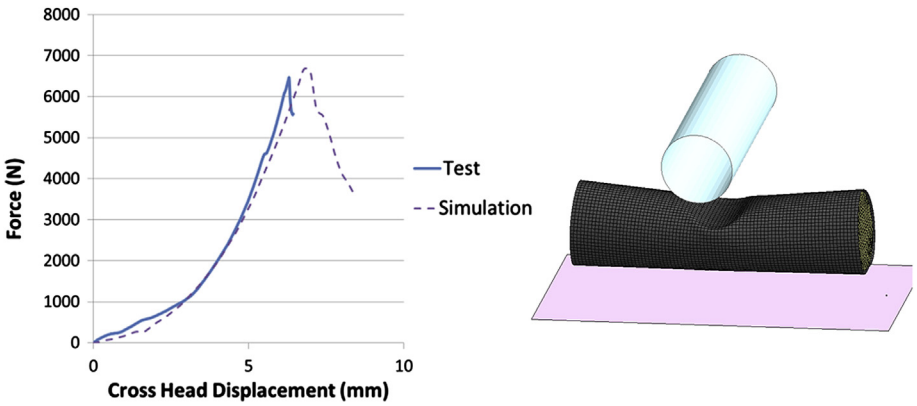

Fig. 13. Comparison of measured and simulated load–displacement curve on 18650 cell under rigid rod indentation.

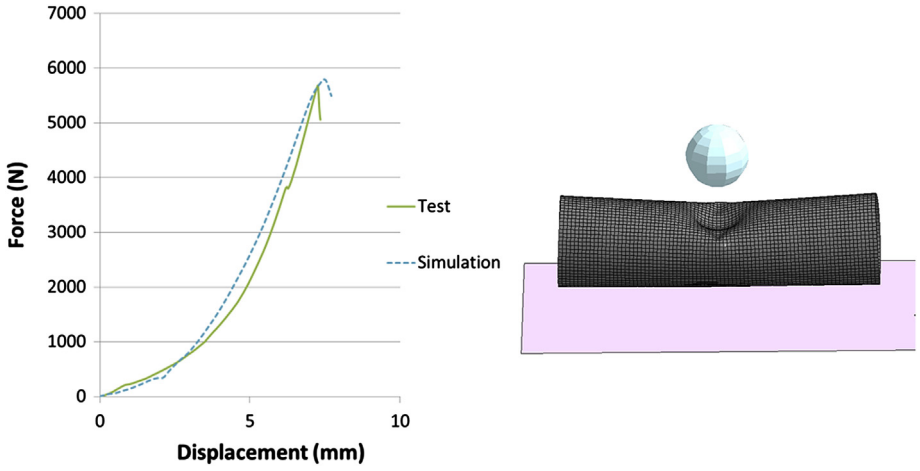

Fig. 14. Comparison of simulated load–displacement curve of 18650 cell under hemispherical punch crush with measured curve.

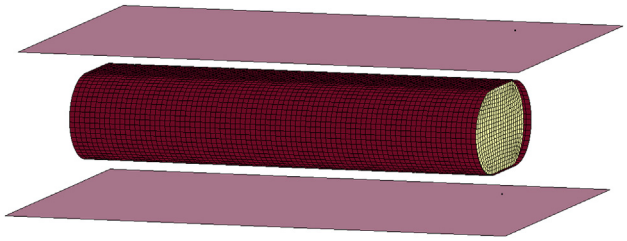

Fig. 15. Finite Element model of the compression between two flat plates.

After calibration of this model, the following material constants were obtained: $\sigma_{\text{yield}} = 0.0003$ GPa, $\sigma_{\text{plateau}} = 0.0006$ GPa, $s = 1000$, $m = 2.7$. When the material constants are substituted in Eq. (38), for $\bar{\varepsilon}^p > 0.02$, the reduces to:

$$R(\bar{\varepsilon}^p) = 0.6 + 600(\bar{\varepsilon}^p)^{2.7} \quad \text{MPa} \tag{39}$$

In uniaxial compression, this function becomes:

$$\sigma = 0.8 + 848(\bar{\varepsilon}^p)^{2.7} \tag{40}$$

It should be noted that under uniaxial compression, the equivalent strain is equal to uniaxial and volumetric strain. The present model uses the concept of a volumetric strain, and the present calibrated stress–strain curve given by Eq. (26) is

$$\sigma = 498(\varepsilon_{\text{av}})^2 \quad \text{MPa} \tag{41}$$

The two models predict very similar stress–strain curve in compression (see Fig. 17).

The small constant term of 0. 8 in Eq. (39) is indistinguishable in the scale of Fig. 17. Therefore, the simplicity of the present model makes it more appealing.

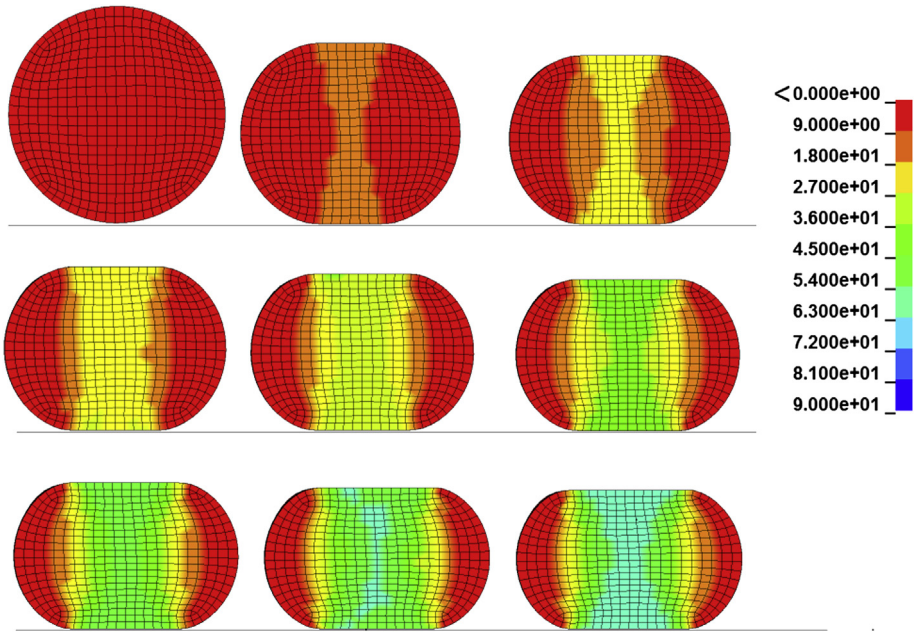

Fig. 16. Progression of buildup a central rectangular compression region, red sections are the areas of no compression/small tension, and the rest of colors show the compressive loads.

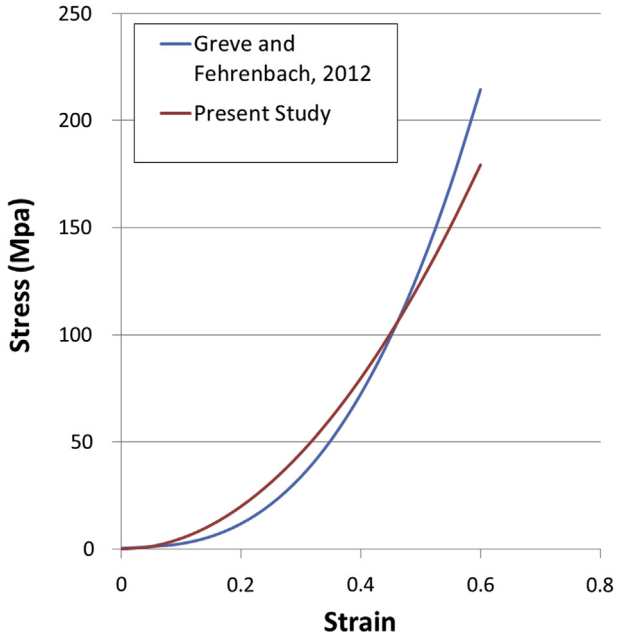

Fig. 17. Comparison of stress–strain relation of the present study and Greve and Fehenbach 2012, under uniaxial compression.

Regarding material failure, Greve and Franbach propose used the Mohr–Columb fracture criteria. On the plane of principal stresses, this criterion takes the form of

$$\sigma_1 - p\sigma_2 = r \tag{42}$$

where p and r are material constants. In the present paper, it is assumed that failure corresponds to a maximum tensile stress value,

$$\sigma_1 = r = \sigma_f \tag{43}$$

referred to as tensile cut-off stress, σ_f (10 MPa). Furthermore, the stress is maintained at the tensile cut-off value until the load bearing capacity of the cross-section is exhausted, and the cell resistance to load suddenly drops. It remains to be seen, under new loading conditions, whether the more general two parameter model, Eq. (42) or the one-parameter model, Eq. (43) should be used to generate correct prediction. In the three typical loading cases of the cylindrical shell, the present simple failure model proved to be adequate.

All the features of the present computational model already exist in LS Dyna, Material Crushable Foam (#60). Therefore, it is available for all the users without a need for developing a user-defined subroutine. At the same time, it is recognized that certain features of the jellyroll cannot be described by the present model. The most important limitation is that the model is isotropic, and therefore, does not account for anisotropic nature of the layered structure of the jellyroll. For example, the tensile forces perpendicular to the layers, which should lead to delamination in the actual cell, will be treated same as tensile forces in the in-plane direction. An extension of the present model to account for structural anisotropy is the subject of the current research of the investigating team.

Acknowledgments

Support of MIT Battery Consortium, as well as Ford_MIT Alliance for this research is greatly appreciated. Authors also acknowledge support of Altair Engineering for providing Hypermesh software.

References

[1] K. Shim, S. Lee, B. Kang, S. Hwang, J. Mater. Process. Technol. 155 (2004) 1935–1942.
[2] P. Liu, E. Sherman, A. Jacobsen, J. Power Sources 189 (2009) 646–650.
[3] A. Sheidaei, X. Xiao, X. Huang, J. Hitt, J. Power Sources 196 (2011) 8728–8734.
[4] G. Venugopal, J. Moore, J. Howard, S. Pendalwar, J. Power Sources 77 (1999) 34–41.
[5] L. Anand, C. Di Leo, MIT Fracture and Battery Workshop (2011).
[6] D. Djian, F. Alloin, S. Martinet, H. Lignier, J. Power Sources 187 (2009) 575–580.
[7] E. Sahraei, J. Campbell, T. Wierzbicki, J. Power Sources 220 (2012) 360–372.
[8] E. Sahraei, R. Hill, T. Wierzbicki, J. Power Sources 201 (2012) 307–321.
[9] E. Sahraei, R. Hill, T. Wierzbicki, Proc. of the Battery Congress (2011).
[10] L. Greve, C. Fehrenbach, J. Power Sources 214 (2012) 377–385.
[11] G. da Costa Machado, M.K. Alves, H.A. Al-Qureshi, R. Rossi, J Brazil Soc Mech Sci Eng (2007) 161–172.
[12] V. Deshpande, N. Fleck, J. Mech. Phys. Solids 48 (2000) 1253–1283.
[13] L.J. Gibson, M.F. Ashby, Cellular Solids: Structure and Properties, Cambridge University Press, 1999.
[14] S. Santosa, T. Wierzbicki, J. Mech. Phys. Solids 46 (1998) 645–669.
[15] S.P. Santosa, T. Wierzbicki, A.G. Hanssen, M. Langseth, Int. J. Impact Eng. 24 (2000) 509–534.
[16] J. Wang, W. Sun, S. Anand, Computat. Mater. Sci. 44 (2008) 195–200.
[17] J. Zhang, N. Kikuchi, V. Li, A. Yee, G. Nusholtz, Int. J. Impact Eng. 21 (1998) 369–386.
[18] Y. Zhang, Y. Tang, G. Zhou, J. Wei, F. Han, Mater. Lett. 56 (2002) 728–731.
[19] E. Sahraei, T. Wierzbicki, in preparation.
[20] J.A. DeRuntz Jr., P.G. Hodge Jr., J. Appl. Mech. 30 (1963) 391.
[21] M. Yahiaoui, PhD Dissertation (1996).